AIAA JOURNAL
Vol. 45, No. 7, July 2007

Electric Charge Buildup in Hypersonic Wind Tunnels with Electron-Beam Energy Addition

M. N. Shneider,* S. O. Macheret,† and R. B. Miles‡
Princeton University, Princeton, New Jersey 08544

DOI: 10.2514/1.16957

A two-dimensional axisymmetric model is developed to predict electric charge and voltage buildup in supersonic/hypersonic nozzle flows of dense air with upstream-propagating high-energy electron beams depositing energy and electric charge into the air. The flowfield and the electron-beam power-deposition profiles were taken from calculations performed elsewhere. The present model includes kinetics of plasma species (electrons, positive ions, and negative ions) and the Poisson equation for electric potential. Both the case of grounded conducting nozzle walls and that of walls covered by a dielectric layer were considered. The model was applied to quantify the important charge and voltage buildup and removal under the conditions expected in medium- and large-scale electron-beam-driven hypersonic wind tunnels.

Nomenclature

c_d	=	effective capacitance per unit length
D_e, D_+, D_-	=	electron, positive ion, and negative ion diffusion coefficients
E	=	electric field strength in the definition of the tunneling detachment, MeV/cm
$\boldsymbol{E}$	=	electric field strength
E_b	=	initial energy of the electron beam
E_d	=	electric field inside the dielectric
E_r	=	radial component of the electric field
E_z	=	longitudinal component of the electric field
e	=	elementary charge
I_b	=	electron-beam current
I_{wall}	=	current to the nozzle wall
$I_{z=L}$	=	current downstream
$I_{z=0}$	=	current into the nozzle throat
k_a	=	three-body attachment rate coefficient
k_d	=	detachment rate coefficient
$\boldsymbol{L}$	=	nozzle length in the z direction
l_d	=	thickness of the dielectric coating
$\dot{m}$	=	mass flow rate
N	=	gas number density
n_e, n_+, n_-	=	electron, positive ion, and negative ion number densities
Q_w	=	negative charge accumulated on the inner dielectric surface per unit length
q_b	=	ionization rate due to the electron beam
q_{power}	=	rate of power deposition, W/m^3
q_t	=	rate at which beam electrons arrive at a given location
R	=	nozzle radius
r	=	radial coordinate
$\tilde{r}$	=	dimensionless radial coordinate
T_e, T	=	electron and ion-molecule temperatures, eV
t	=	time
V_d	=	voltage on the dielectric sheath
$V_{\max}$	=	peak electric potential inside the nozzle
Y_i	=	cost of ionization
z	=	longitudinal coordinate
$\tilde{z}$	=	dimensionless longitudinal coordinate
α	=	electric-field-dependent Townsend ionization coefficient
β_{dr}	=	dissociative recombination rate coefficient
β_{ii}	=	ion–ion recombination coefficient
β_{3e}	=	three-body recombination rate coefficients with an electron as the third body
β_{3M}	=	three-body recombination rate coefficients with a molecule as the third body
Γ_e, Γ_+, Γ_-	=	electron, positive ion, and negative ion fluxes
ε_d	=	relative dielectric permittivity
ε_0	=	permittivity of vacuum
ε_-	=	electron affinity, eV
μ_e, μ_+, μ_-	=	electron, positive ion, and negative ion mobilities
ρ_0	=	atmospheric density at STP
ρ	=	gas density
τ_f	=	lifetime of the negative ion in the electric field E due to the tunneling detachment, s
φ	=	electric potential

Presented as Paper 4035 at the 34th AIAA Plasmadynamics and Lasers Conference, Orlando, FL, 23–26 June 2003; received 3 April 2005; revision received 21 February 2007; accepted for publication 9 March 2007.

*Research Scientist, Department of Mechanical and Aerospace Engineering, D-414 Engineering Quadrangle; shneyder@princeton.edu. Senior Member AIAA.

†Currently Senior Staff Aeronautical Engineer, Lockheed Martin Aeronautics Company, Skunk Works, 1011 Lockheed Way, Palmdale, CA, 93599-0160; sergey.macheret@lmco.com. Associate Fellow AIAA.

‡Professor, Department of Mechanical and Aerospace Engineering, D-414 Engineering Quadrangle; miles@princeton.edu. Fellow AIAA.

I. Introduction

IN AN innovative concept of hypersonic wind tunnels that is currently being developed, large amounts of energy would be deposited into highly compressed (to hundreds and thousands of atmospheres) air as this air expands in a supersonic nozzle; the expansion would allow conversion of the deposited energy into kinetic energy of the flow while keeping static temperature at a relatively low level [1].

High-power (megawatt-level) relativistic (electron energy of several mega electron volts) electron beams represent an attractive way of adding energy to the supersonic flow of dense air. The beams would be directed upstream, guided and focused by strong magnetic fields. As shown previously at Princeton University and Sandia National Laboratories, with a proper arrangement, most of the energy deposition would occur in a 10–20-cm-long region of the nozzle, and the radial profile of energy-deposition rate would resemble a "top hat," with a uniform energy-deposition rate in the core flow and very little power loss into the wall [2,3].

When an electron beam is injected into the nozzle, the beam not only heats and ionizes the gas, but it also brings a negative space charge. If the beam-induced electrical conductivity is sufficiently high, the space charge will be removed by the electric current to the grounded walls and also downstream, toward the beam-injection region. At steady state, a negative potential will exist in the region in which the maximum beam-energy deposition occurs. If this negative potential is comparable with the initial energy (voltage) of the beam, then the heating profile would shift downstream, thus altering the enthalpy addition and the exit-flow parameters.

Thus, in the present paper, we present results of a modeling effort that was undertaken to quantify the important charge buildup and removal under the conditions expected in electron-beam-driven hypersonic wind tunnels.

II. Model

Axisymmetric (i.e., dependent on the radial coordinate r and the axial coordinate z) profiles of gas density, temperature, and velocity, nozzle contours, and top-hat electron-beam energy-deposition profiles were used for the two cases: 1-MW, 800-keV experiments underway at Sandia National Laboratories [2], and a planned 200MW, 3-MeV medium-scale hypersonic wind tunnel (MSHWT) [3]. The electron-beam energy-addition profiles were computed using the CYLTRAN code developed at Sandia National Laboratories. Note that the steady-state, viscous, axisymmetric, real-gas fluid dynamics coupled with electron-beam energy addition was modeled assuming no charge-buildup effects. The calculated flowfield and electron-beam power-deposition profiles were then used in the charge-buildup modeling.

For the present work, a new code was developed. The time-accurate axisymmetric code includes plasma kinetics and the Poisson equation for the electric field. Equations for electrons and both positive and negative ions include the electron source due to the beam injection, gas ionization by beam electrons, ionization by plasma electrons for which the temperature is determined by the local electric field and gas density, drift and diffusion transport of charged particles, electron attachment to oxygen, collisional (thermal) electron detachment from negative ions, collisionless (tunneling) electron detachment from negative ions, dissociative recombination of electrons and positive ions, three-body electron-ion recombination with an electron as the third body, three-body electron–ion recombination with a molecule as the third body, and mutual recombination of positive and negative ions. Rate coefficients of these processes were taken from the literature [4–6] and will be given later in the paper. The rate coefficient of ion–ion recombination was generalized in this work to encompass a very wide range of pressures and temperatures expected in the electron-beam-driven hypersonic wind tunnels.

The kinetics of charged particles and electrical current conduction are described by the following equations:

$$\frac{\partial n_e}{\partial t} + \mathrm{div}\Gamma_e = q_b + q_t + \alpha|\Gamma_e| - \beta_{\mathrm{dr}} n_e n_+ - \beta_{3e} n_e^2 n_+ - \beta_{3M} n_e n_+ N - k_a n_e (0.2N)^2 + k_d n_- (0.2N) + n_-/\tau_f$$

$$\frac{\partial n_+}{\partial t} + \mathrm{div}\Gamma_+ = q_b + \alpha|\Gamma_e| - \beta_{\mathrm{dr}} n_e n_+ - \beta_{3e} n_e^2 n_+ - \beta_{3M} n_e n_+ N - \beta_{\mathrm{ii}} n_+ n_-$$

$$\frac{\partial n_-}{\partial t} + \mathrm{div}\Gamma_- = k_a n_e (0.2N)^2 - k_d n_- (0.2N) - \beta_{\mathrm{ii}} n_+ n_- - n_-/\tau_f$$

$$\Gamma_{e,-} = -\mu_{e,-} n_{e,-} \boldsymbol{E}(r,z) - D_{e,-} \nabla n_{e,-} \qquad \Gamma_+ = \mu_+ n_+ \boldsymbol{E}(r,z) - D_+ \nabla n_+$$

$$\mathrm{div}\Gamma = \frac{\partial \Gamma_r}{\partial r} + \frac{\Gamma_r}{r} + \frac{\partial \Gamma_z}{\partial z} \qquad D_e = \mu_e T_e; \qquad D_{+,-} = \mu_{+,-} T \tag{1}$$

In Eq. (1), $0.2N$ is the number density of oxygen molecules (assuming that molecular oxygen mole fraction is 0.2), β_{3e} and β_{3M} use electron e or a molecule M as the third body, $k_a = e + \mathrm{O_2} + \mathrm{O_2} \rightarrow \mathrm{O_2^-} + \mathrm{O_2}$, and $k_d = O_2^- + O_2 \rightarrow e + O_2 + O_2$.

The Poisson equation for electric potential coupled with plasma kinetics is

$$\Delta\varphi = \frac{\partial^2 \varphi}{\partial z^2} + \frac{1}{r}\frac{\partial}{\partial r}\left(r\frac{\partial \varphi}{\partial r}\right) = -\frac{e}{\varepsilon_0}(n_+ - n_e - n_-) \qquad \boldsymbol{E}(r,z) = -\mathrm{grad}\varphi \tag{2}$$

The boundary conditions are

$$\varphi_{R(z)} = 0, \qquad \left.\frac{\partial \varphi}{\partial r}\right|_{r=0} = 0, \qquad \left.\frac{\partial \varphi}{\partial z}\right|_{z=0} = \left.\frac{\partial \varphi}{\partial z}\right|_{z=0+\Delta z} \qquad \left.\frac{\partial \varphi}{\partial z}\right|_{z=L} = \left.\frac{\partial \varphi}{\partial z}\right|_{z=L-\Delta z} \tag{3}$$

where $R(z)$ is the nozzle radius. The nozzle wall is assumed to be grounded.

The ionization rate by electron beam is calculated as $q_b = q_{\mathrm{power}}/eY_i$, where q_{power} is obtained from CYLTRAN and fluid dynamic computations [3], and $Y_i = 34$ eV is the cost of ionization. The rate at which beam electrons arrive at a given location is calculated as

$$q_t(r,z) = \frac{(I_b/e) q_b(r,z)}{2\pi \int_0^L \int_0^{R(z)} r q_b(r,z)\, \mathrm{d}r\mathrm{d}z} \tag{4}$$

Equation (4) assumes that the normalized rate of electron addition in a given volume element is proportional to the normalized rate of heating in that element. What justifies this approximation is the very high gas density that translates into a very short relaxation length for low-energy electrons. Indeed, in the 1-MW case, the gas density in the energy-addition region ranges from about 1 (at the exit) to about 50 (at the entrance) normal atmospheric densities, and in the 200-MW case, the gas-density range is 10–800 normal atmospheric densities. The relaxation length for 1-keV electrons is only 40 μm, even at normal atmospheric density, and this length decreases with the decrease in electron energy and increase in gas density.

The rate coefficients in Eq. (1) are [4–6]

$$\beta_{\mathrm{dr}} = 4 \times 10^{-7} \times (300/T_e)^{1.5}\ \mathrm{cm^3/s} \quad \text{for } \mathrm{NO^+} + e \rightarrow \mathrm{N} + \mathrm{O}$$

$$\beta_{\mathrm{dr}} = 1.3 \times 10^{-6} \times (300/T_e)^{0.5}\ \mathrm{cm^3/s}$$

for $\mathrm{NO^+} \cdot (\mathrm{NO}, \mathrm{N_2}, \mathrm{O_2}) + e \rightarrow \mathrm{NO} + \mathrm{NO}, \mathrm{N_2}, \mathrm{O_2}$

or $\mathrm{O_4^+} + e \rightarrow \mathrm{O_2} + \mathrm{O_2}$

$$\beta_{3e} = 10^{-19} \times (300/T_e)^{4.5}\ \mathrm{cm^6/s}$$

$$\beta_{3M} = 6 \times 10^{-27} \times (300/T_e)^{1.5}\ \mathrm{cm^6/s}$$

$$k_a = 1.4 \times 10^{-29} \times \frac{300}{T_e} \times \exp\left(\frac{100}{T} - \frac{700}{T_e}\right)\ \mathrm{cm^6/s}$$

$$k_d = 2.7 \times 10^{-10} \times (T/300)^{0.5} \times \exp(-5590/T)\ \mathrm{cm^3/s}$$

$$\beta_{\mathrm{ii}} = 2 \times 10^{-25} \times (300/T)^{2.5} \times N\ \mathrm{cm^3/s} \quad \text{if } \rho < \rho_0 \times (T/300)^{1.5}$$

$$\beta_{\mathrm{ii}} = 5.374 \times 10^{-6} \times (\rho_0/\rho)\ \mathrm{cm^3/s} \quad \text{if } \rho \geq \rho_0 \times (T/300)^{1.5}$$

The lifetime of negative ion in the electric field E due to the tunneling detachment is [7]

$$\tau_f = -13.17 + \tfrac{1}{2}\lg \varepsilon_- - \lg E + 29.67\varepsilon_-^{3/2}/E$$

where $\varepsilon_- \approx 0.5$ eV. In the two computed cases, the tunneling detachment turned out to be negligible due to the relatively low magnitudes of electric field.

Air-plasma transport coefficients (mobilities and diffusion coefficients), dependent on E/N, as well as the electron temperature as a function of E/N, were taken from the literature [5,8].

If during the evolution of the electric field, the ratio of electric field strength and the gas number density, E/N, locally reaches the threshold value of 110 $Td = 1.1 \times 10^{-15}$ V · cm^2, electric breakdown (spark) will ensue at this location. In such a case, the model would need to be complemented by a spark model. However, in both computed cases, E/N never reached the breakdown threshold, thus making additional spark modeling unnecessary.

Computations were performed on a rectangular grid $\tilde{z}$, $\tilde{r} \in [0, 1]$, where the dimensionless coordinates are $\tilde{r} = r/R(z)$ and $\tilde{z} = z/L$. The drift-diffusion equations for charge-particle balance [Eq. (1)] are of the mixed, rather than strictly hyperbolic, type; however, they are near hyperbolic due to the small magnitude of the Townsend ionization term. Therefore, very reliable algorithms developed in fluid dynamics can be used. In this work, the second-order McCormack method [9] was used. At each time step, the Poisson equation (2) was solved by the implicit successive over-relaxation method [9] for the instantaneous charge-density distribution.

III. Results

A. Nozzle with Conducting Walls

The results for the 1-MW case with a 800-keV electron beam are shown in Figs. 1–5. The stagnation pressure and temperature in this case are 17.92 MPa and 650 K, respectively, and the mass flow rate is $\dot{m} \approx 2.61$ kg/s. The approximate range of the flow velocity in the energy-deposition region is 500–800 m/s, and the approximate ranges for gas density, static temperature, and static pressure are 1–50 kg/m^3, 400–1000 K, and 1–20 MPa, respectively. Figure 1 shows the time evolution of the peak electric potential inside the nozzle and the electric currents into the wall and downstream (into the isentropic expansion region). The electric current upstream (into the nozzle throat) is not shown in Fig. 1, because it turned out to be small compared with both I_{wall} and $I_{z=L}$. The absolute values of the currents were computed as

$$I_{\text{wall}} = 2e\pi \int_0^L R(z)\{\Gamma_e[R(z), z] + \Gamma_-[R(z), z]\}\,\mathrm{d}z$$

and

$$I_{z=0,z=L} = 2e\pi \int_0^{R(z)} r[\Gamma_e(r, z) + \Gamma_-(r, z)]\mathrm{d}r$$

As seen in Fig. 1, in about 1 μs from the start, the peak potential reaches a steady-state value of about 3 kV, $I_b = 1.25$ A is balanced by the current into the wall, and charge removal both upstream and downstream of the computational domain is negligible. Note that grid independence was checked by changing the number of grid points by a factor of 2 in each (radial and axial) dimension; as seen in Fig. 1, the results are practically unchanged.

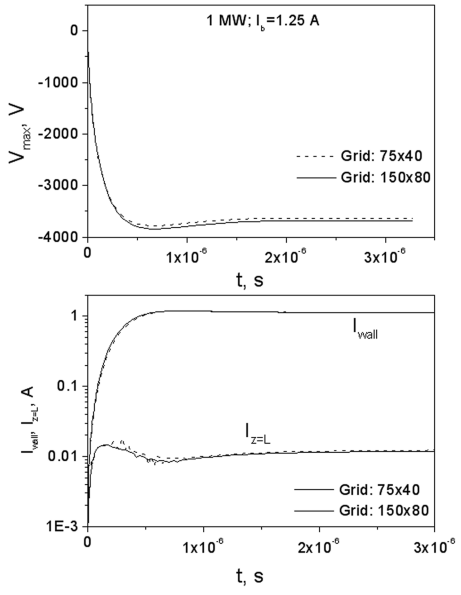

Fig. 1 Time evolution of the peak electric potential inside the nozzle, the electric currents into the wall, and downstream (into the isentropic expansion region); beam energy is $\varepsilon_b = 0.8$ MeV.

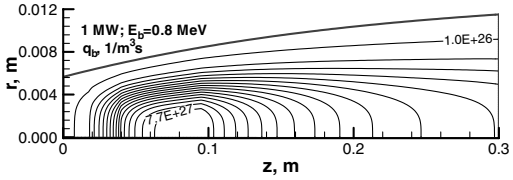

Fig. 2 Steady-state contours of electron-beam-induced ionization rate in the case of Fig. 1; the interval between the contour lines corresponds to 5.07×10^{26} 1/m^3 · s.

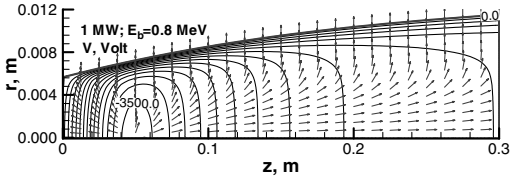

Fig. 3 Steady-state contours of electric potential (solid lines) and the electron and negative-ion current flow lines with respect to the gas (arrows) in the case of Fig. 1; the interval between the contour lines corresponds to 250 V.

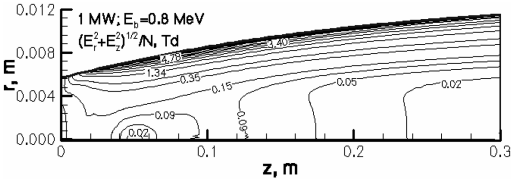

Fig. 4 Steady-state contours of E/N, in Td (10^{-17} V · cm^2), in the case of Fig. 1.

Figures 2–4 show the steady-state contours of ionization rate, potential, and the E/N parameter. Figure 3 clearly shows the region in which negative space charge and potential is concentrated. In the same figure, arrows show the directions of charge removal. Figure 4 shows that the values of E/N are very low everywhere: one–three orders of magnitude below those in glow and RF discharges in the air.

As seen in Fig. 5, which depicts steady-state number densities of charged species, number densities of positive and negative ions are

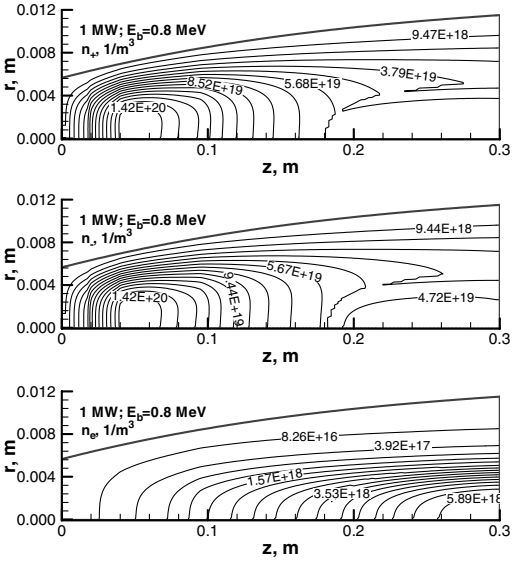

Fig. 5 Steady-state contours of the number densities of positive ions, negative ions, and electrons in the case of Fig. 1.

almost equal to each other, whereas the electron density is much lower due to attachment. Note that the balance of charged particles is dominated by attachment and ion–ion recombination, which establish the quasi-steady-state number densities on a nanosecond timescale. With the flow velocity on the order of 10^3 m/s, the convective removal of charged species is thus negligible, which justifies the omission of convective terms in the balance equations (1). The axial convective velocity can be comparable with the electron and, especially, ion axial-drift velocities; however, because the axial current was found to be much smaller than the current to the wall, the convective motion of charged species does not contribute significantly to the total current.

Overall, the results for the 1-MW case show that the steady-state negative potential, 3 kV, is much lower than the beam voltage of 800 kV, due to the charge removal into the grounded nozzle wall. Thus, charge buildup is not expected to significantly affect the 1-MW experiment.

Figures 6–10 show the computed results for the MSHWT (200 MW, $\varepsilon_b = 3$ MeV, and $I_b = 66.6$ A). The stagnation pressure and temperature in this case are 2300 MPa and 750 K, respectively,

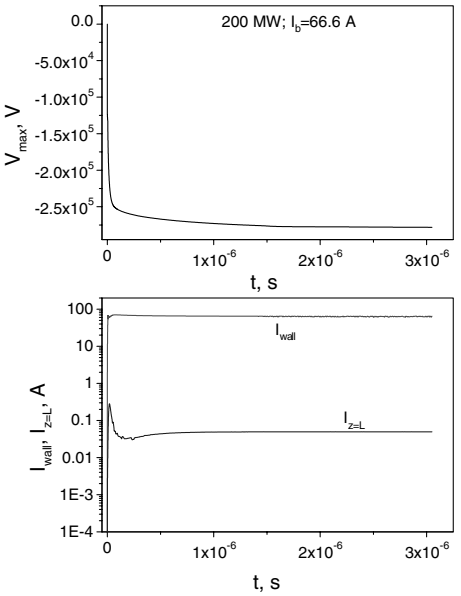

Fig. 6 Time evolution of the peak electric potential inside the nozzle, and the electric currents into the wall and downstream (into the isentropic expansion region); beam energy is $\varepsilon_b = 3$ MeV.

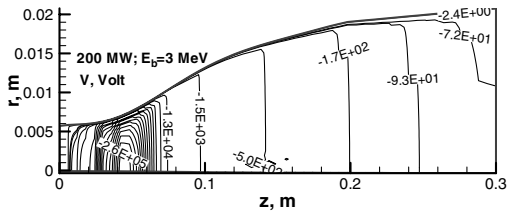

Fig. 7 Contours of electric potential at $t = 3 \times 10^{-6}$ s in the case of Fig. 6.

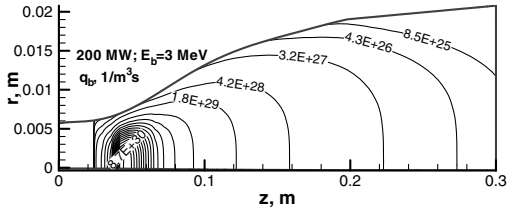

Fig. 8 Contours of electron-beam-induced ionization rate at $t = 3 \times 10^{-6}$ s in the case of Fig. 6.

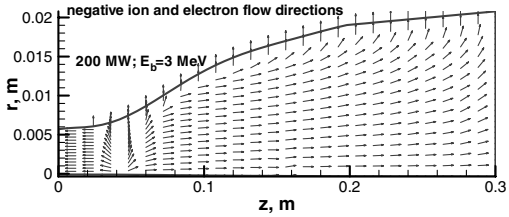

Fig. 9 Flow directions of electrons and negative ions with respect to the gas at $t = 3 \times 10^{-6}$ s in the case of Fig. 6.

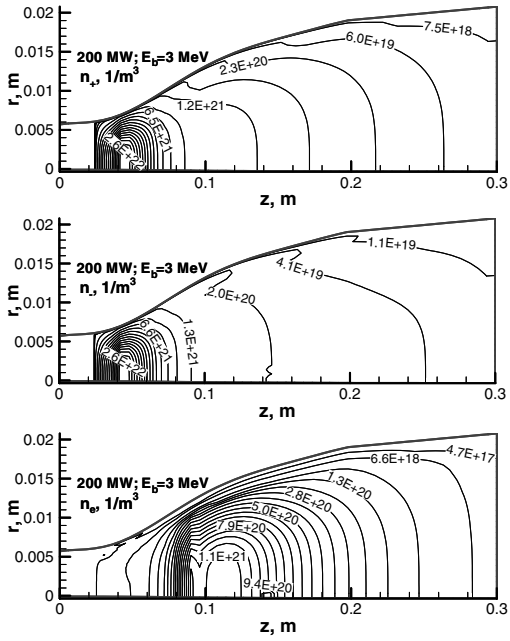

Fig. 10 Contours of number densities of negative ions, positive ions, and electrons at $t = 3 \times 10^{-6}$ s in the case of Fig. 6.

and the mass flow rate is $\dot{m} \approx 167.15$ kg/s. The approximate range of the flow velocity in the energy-deposition region is 2000–2500 m/s, and the approximate ranges for gas density, static temperature, and static pressure are 10–800 kg/m^3, 1000–3000 K, and 10–125 MPa, respectively.

As seen in Fig. 6, the charge brought by the electron beam is also removed by the conduction current into the grounded wall, as in the previous (800 kV, 1 MW) case. However, because of the much higher electron-beam current, a significantly higher steady-state negative potential (about 0.28 MV, or almost 10% of the initial beam voltage) is needed to provide the charge removal into the wall in this case. Note also that due to the high static temperatures of up to 3000 K, substantial electron detachment from negative ions occurs, so that at $z \geq 0.1$ m, the number density of electrons is comparable with or greater than that of negative ions.

B. Nozzle with Insulated Walls

If the nozzle walls are covered by a dielectric sheath with relative dielectric permittivity and thickness (Fig. 11), the negative charge injected by the beam can accumulate inside the nozzle, charging the capacitor distributed along the walls. The effective capacitance per unit length is

$$c_d(z) = \frac{2\pi R(z)\varepsilon_0\varepsilon_d}{l_d} \text{ F/m}$$

The negative charge accumulated on the inner dielectric surface per unit length is

$$Q_w(z,t) = -2\pi e R(z) \int_0^t \{\Gamma_{-,r}[z, R(z), t] + \Gamma_e[z, R(z), t]\}\, dt \text{ C/m}$$

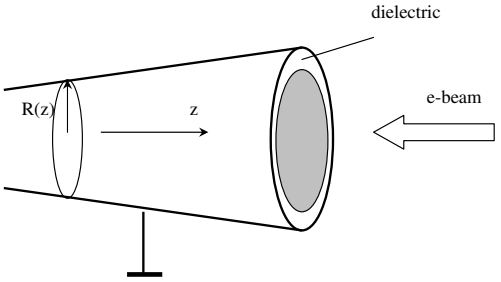

Fig. 11 Schematic of a nozzle with the walls covered by dielectric.

The voltage on the dielectric sheath is $V_d(z,t) = Q_w(z,t)/c_d(z)$ V. The electric field inside the dielectric is

$$E_d(z,t) = \frac{V_d(z,t)}{\varepsilon_d l_d} \text{ V/m}$$

Computations were performed for the 1-MW case and the nozzle walls covered by a dielectric layer with $\varepsilon_d = 5$ and $l_d = 1$ mm.

In this case of insulated walls, we observed continuous growth of the amplitude of potential inside the nozzle (Figs. 12 and 13, upper plot) and also a continuously increasing electric field in the dielectric layer (Fig. 13, bottom plot). This process can be stopped when the breakdown threshold is reached in the dielectric layer or downstream in the gas. At the conditions of this specific case, a dielectric breakdown can happen first at $z = 0.1$ m (Fig. 13, bottom plot).

IV. Conclusions

When developing hypersonic wind tunnels with electron-beam energy addition in the supersonic nozzle, it is important to understand the possible effects of accumulation and removal of negative electric potential in the energy-addition region. If the potential is comparable with the initial energy of beam electrons, then the injected electrons will be repulsed downstream, resulting in a substantially altered energy-addition profile and flow parameters. This issue was addressed in the present paper on the basis of a 2-D time-accurate model that included plasma kinetics and the Poisson equation.

In the case of metallic grounded nozzle walls, the electron-beam-induced electrical conductivity is sufficiently high for the space charge to be efficiently removed by the electric current to the grounded walls. In the case with a 0.8-MeV, 1-MW electron beam, the steady-state negative potential turned out to be negligible compared with the electron-beam energy, and the influence of this potential on the heating profile in the nozzle should be insignificant. However, in the case with a high-power electron beam (200 MW, 3 MeV), the steady-state negative potential in the nozzle turned out to be 0.28 MV, or about 10% of the initial electron-beam voltage. This negative potential can affect the beam propagation and energy-deposition profile, which would change the exit flow. Thus, a coupled analysis of charge buildup, electron-beam propagation, and fluid dynamics will be desirable in the high-power case.

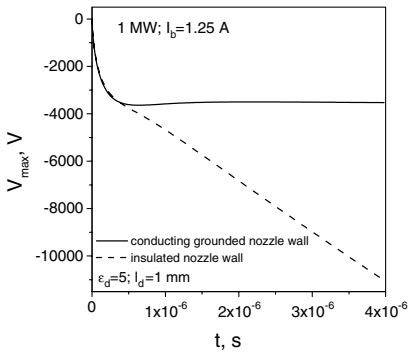

Fig. 12 Time evolution of the peak electric potential inside the nozzle.

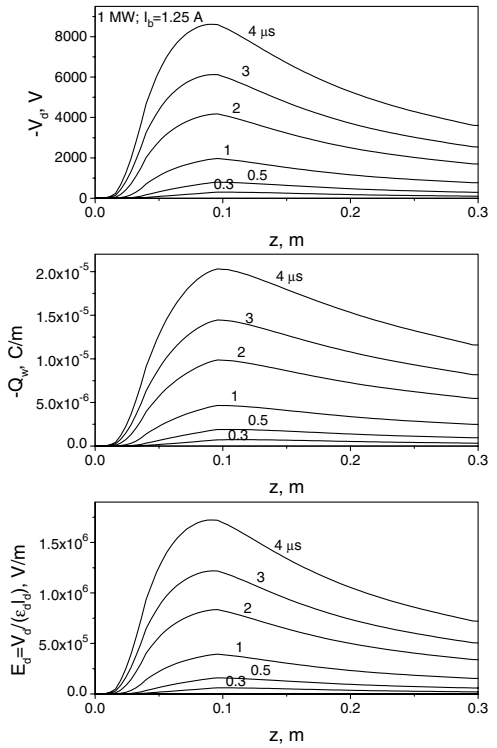

Fig. 13 Longitudinal profiles of the voltage drop on the dielectric layer (upper plot), negative charge on the dielectric wall (middle plot), and the electric field inside the dielectric (bottom plot).

The charge buildup was predicted to be very high, even in the 0.8-MeV, 1-MW case, if the walls are covered by a dielectric layer. In this case, the negative potential can reach high values and is limited only by electric breakdown of the dielectric layer or of the gas downstream of the peak energy-deposition region.

Note that in the present modeling, we disregarded UV, VUV, and x rays generated by relativistic electron beams interacting with dense air and the walls. The high-energy photons can detach electrons from negative ions, thus increasing the conductivity and decreasing the charge buildup. These phenomena can be studied in the future.

Acknowledgments

This work was supported by the Mariah II Wind Tunnel Project with funding from the U.S. Air Force Arnold Engineering Development Center in conjunction with MSE Technology Applications, Inc. We are also grateful to Ihab Girgis of Princeton University for providing his results of 2-D modeling of fluid dynamics coupled with electron-beam energy addition.

References

[1] Miles, R., Brown, G., Lempert, W., Yetter, R., Williams, G. J., Bogdonoff, S. M., Natelson, D., and Guest, J. R., "Radiatively Driven Hypersonic Wind Tunnel," *AIAA Journal*, Vol. 33, No. 8, 1995, pp. 1463–1470.

[2] Mansfield, D., Miles, R., Brown, G., Howard, P., Lipinski, R., and Girgis, I., "A 1 MW Electron Beam Heated Radiatively Driven Wind Tunnel Experiment," AIAA Paper 2002-3130, June 2002.

[3] Girgis, I. G., Brown, G. L., Miles, R. B., and Lipinski, R. J., "Fluid Mechanics of a Mach 7–12 Electron Beam Driven Missile Scale Hypersonic Wind Tunnel—Modeling and Predictions," *Physics of Fluids*, Vol. 14, No. 11, 2002, pp. 4026–4039.

[4] Kossyi, I., Kostinsky, A. Yu., Matveyev, A. A., and Silakov, V. P., "Kinetic Scheme of the Non-Equilibrium Discharge in Nitrogen-Oxygen Mixtures," *Plasma Sources Science and Technology* , Vol. 1, No. 3, 1992, pp. 207–220.

[5] Raizer, Yu. P., *Gas Discharge Physics*, Springer, Berlin, 1991.

[6] Macheret, S. O., Shneider, M. N., and Miles, R. B., "Modeling of Air Plasma Generation by Repetitive High-Voltage Nanosecond Pulses," *IEEE Transactions on Plasma Science*, Vol. 30, No. 3, 2002, pp. 1301–

1314.
[7] Demkov, Yu. N., and Drukarev, G. F., "Decay and Polarizability of Negative Ions in an Electric Field," *Soviet Physics, JETP*, Vol. 20, No. 3, 1965, pp. 61–618.
[8] *Handbook of Physical Quantities*, edited by I. S. Grigoriev, and E. Z. Meilikhov, CRC Press, Boca Raton, FL, 1997, Chap. 20.
[9] Anderson, D. A., Tannehill, J. C., and Pletcher, R., *Computational Fluid Mechanics and Heat Transfer*, Hemisphere, New York, 1984.

D. Gaitonde
Associate Editor